

Article

Hybrid Electromagnetic and Triboelectric Nanogenerators with Multi-Impact for Wideband Frequency Energy Harvesting

Jianxiong Zhu ^{1,2,*}, Aochen Wang ¹, Haibing Hu ³  and Hua Zhu ⁴

¹ Beijing Institute of Nanoenergy & Nanosystems, Chinese Academy of Sciences, National Center for Nanoscience and Technology (NCNST), Beijing 100083, China; wangaochen@binn.cas.cn

² Department of Mechanical Engineering, Korea Advanced Institute of Science and Technology (KAIST), 291 Daehak-ro, Yuseong-gu, Daejeon 34141, Korea

³ Academy of Photoelectric Technology, Hefei University of Technology, Hefei 230009, China; huhb@hfut.edu.cn

⁴ Department of Mechanical and Aerospace Engineering, University of Missouri, Columbia, MO 65211, USA; hzcn3@mail.missouri.edu

* Correspondence: simonzhu@kaist.ac.kr; Tel.: +82-10-2803-9249

Received: 3 November 2017; Accepted: 28 November 2017; Published: 1 December 2017

Abstract: We present a hybrid electromagnetic generator (EMG) and triboelectric nanogenerator (TENG) using a multi-impact approach for broad-bandwidth-frequency (10–45 Hz) energy harvesting. The TENG and the EMG were located at the middle and the free end of the cantilever beam, respectively. When the system was subjected to an external vibration, the cantilever beam would be in a nonlinear response with multiple impacts from a low frequency oscillator. The mathematical model included a TENG oscillator which can have multiple impacts on the cantilever, and the nonlinear Lorenz force which comes from the motion of the coil in the electromagnetic field. Due to the strong nonlinearity of the impacts from the TENG oscillator and the limited space for the free tip of the cantilever, the dynamic response of the cantilever presented a much broader bandwidth, with a frequency range from 10–45 Hz. We also found that the average generated power from TENG and EMG can reach up to $30 \mu\text{W}/\text{m}^2$ and $53 \mu\text{W}$, respectively. Moreover, the dynamic responses of the hybrid EMG and TENG were carefully analyzed, and we found that the measured experimental results and the numerical simulations results were in good agreement.

Keywords: electromagnetic and triboelectric harvester; multi-impact; PTFE film; frequency up-conversion; nonlinear dynamic response

1. Introduction

Harvesting vibration energy to power low power electronics has attracted extensive interest in the last decade. Compared with the obtained power from conventional chemistry batteries, energy harvesting technology incorporated into a system has tremendous advantages in our everyday life due to operation with much longer life times and an environmentally friendly nature. Vibration-to-electrical transformation using piezoelectric, electrostatic, triboelectric, and electromagnetic principles has been investigated for energy harvesting [1–8]. When compared with the principle using piezoelectric or electrostatic in device, electromagnetic or triboelectric methods benefit from a simple structure and a high electrical performance output. It was demonstrated that an electromagnetic or triboelectric device can reach up to several milliwatts of power, whereas the piezoelectric or electrostatic method can only generate several microwatts of power [9,10]. Typically, when the frequency of the external excitation is close to the resonant frequency of the self-powered device, the self-powered device operates very

well. Whereas the external frequency is beyond a narrow band of the resonant frequency, almost no output power comes out from the self-powered device due to its limited response. Thus, operation at a narrow bandwidth presents a major limitation because of the vibration environment in our daily life more often wide range and low frequency of daily life [11–13]. Challa et al. [12] first conducted impact vibration research, and they designed a resonant energy harvester involving the impact of a free cantilever beam. After that, some other groups proposed using nonlinearity to broaden the frequency bandwidth so that nonlinear bi-stable springs were able to harden or soften the suspensions for widen the bandwidth of the harvesters [14–17]. Abed et al. introduced a multi-modal vibration energy harvesting approach based on arrays of coupled levitated magnets and, by this method, harvested the vibration energy in the operating frequency range of 4.6–14.5 Hz, with a bandwidth of 190% and a normalized power [14]. Park et al. reported a dual Halbach array and a magnetic spring system for a maximum average power of 1093 μW with a 44 Ω load, 11 Hz, and 0.5 g acceleration [18].

Recently, hybrid nanogenerators combining several mechanisms, such as the use of piezoelectric and triboelectric principles to convert mechanical energy into electricity, have been attracting an increasing amount of attention, [10,18–30]. Mahmoudi et al. reported a multiphysics hybrid piezoelectric–electromagnetic vibration energy harvester with a nonlinear equation of motion for an enhancement power density up to 84% [20]. Zhang et al. introduced a water-proof triboelectric–electromagnetic generator in a harsh environment, which can harvest enough power to light LED light [21]. However, the low frequency constrained the power density out from EMG in their design. Zhang et al. reported a hybrid piezoelectric and triboelectric mechanisms harvester [22]. However, the output power from their device presented with a narrow bandwidth which constrained the potential application. Guo et al. took advantage of the electromagnetic induction and triboelectricity principles for a motion sensor. The goal of their research focused on the self-powered motion sensing [10]. Zhang et al. reported a hybridized electromagnetic triboelectric nanogenerator for wearable electronics [27]. Their designed prototype was driven by substantial motion force, which was not suitable for low vibration energy harvesting. Here, we propose a hybrid electromagnetic generator (EMG) and triboelectric nanogenerator (TENG) using multiple impacts for broad-bandwidth-frequency (10–45 Hz) energy harvesting. Due to the nonlinearity of the impact and the constraint space, the dynamic response of the cantilever presented a much broader bandwidth with two peaks (20 Hz and 30 Hz) between its oscillator resonant frequencies and several times of the oscillator resonant frequencies.

2. System and Design

As shown in Figure 1a,b, the hybrid system consists of a copper pick-up coil, a piece of copper impact sheet located at the bottom of the polydimethylsiloxane (PDMS) blocks, an acrylic cantilever beam, a polytetrafluoroethylene (PTFE)/carbon black (CB) film, and a circular shape permanent magnetic. Five milliliters of silicone rubber (Smooth-On Ecoflex 00-30, Smooth-on company, Macungie, PA, USA) and 5 mL of carbon black power (TIMCAL Super P[®] Conductive Carbon Black, TIMCAL Graphite & Caron Company, Bodio, Switzerland) were added into a cup with the aid of mechanical stirring for 30 min for a compound conductive CB film. The resonant frequency of the acrylic cantilever was calculated around 74.5 Hz via FEM (COMSOL Multiphysics[®], version 4.4, COMSOL company, Burlington, MA, USA) (See Figure 1b). A circular permanent NdFeB magnet 1 cm in diameter was placed 2 mm below the free tip of acrylic cantilever. The pick-up coil was made of 36 gauge copper wire with an effective space area of 78.5 mm². The cantilever clamped at one side, and the other side was free to vibrate with a much higher frequency than the excitation frequency. The copper impact mass had a weight of 2 g, and it was used to improve the momentum transfer to the high frequency cantilever. The PDMS bar was designed to resonate at 8 Hz. The low frequency PDMS bar was able to repeat triboelectric impacts to the PTFE/CB compound film onto the high frequency cantilever beam. To clearly show the electrical performance of TENG, the oscillator and the cantilever had a close contact. The repeated impacts starting with a low frequency enabled the frequency up-conversion to match

a much higher frequency of the cantilever beam. Note that the PTFE film was corona charged (high voltage polarization apparatus, Model ET-2673A, Entai company, Nanjing, China) at room temperature for 5 min with the voltages of -6.50 kV. X-ray diffraction (XRD, X'pert powder brand, manufactory, Panalytical company, Almelo, The Netherlands) shown in Figure 1c was used to demonstrate the PTFE film material. The XRD pattern showed an intense peak centered at $2\theta = 18.06^\circ$, indicating a long-range order in the (100) lattice plane and a typically PTFE crystalline structure. The peak at $2\theta = 31.62^\circ$ was indexed to (100) reflection, which was associated with an in-plane structure. The Raman spectrum of mixture composite (see Figure 1d) depicts a substantial peak at 743.5 cm^{-1} , which demonstrated PTFE materials. The surface morphology of the PTFE film was characterized by a SEM equipment (Hitachi SU-8010, Hitachi company, Tokyo, Japan) shown in Figure 2. The goal of these two figures was to describe the roughness of the PTFE tribo-contact surface.

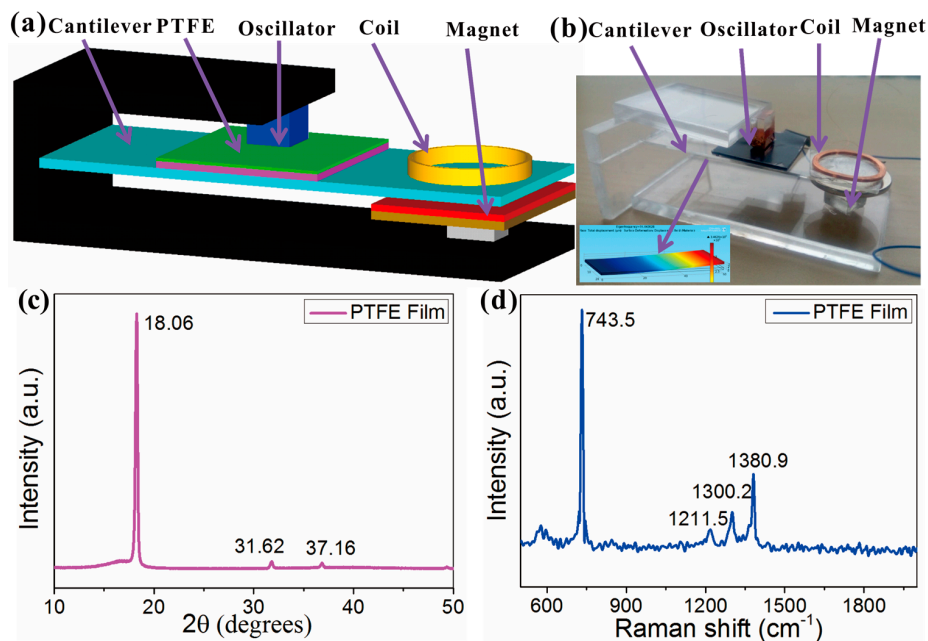


Figure 1. 3D schematic view of the hybrid EMG and TENG multi-impact energy harvester: (a) 3D-view schematic graph; (b) a prototype; (c) wide angle X-ray diffraction pattern of PTFE; (d) Raman spectra of PTFE.

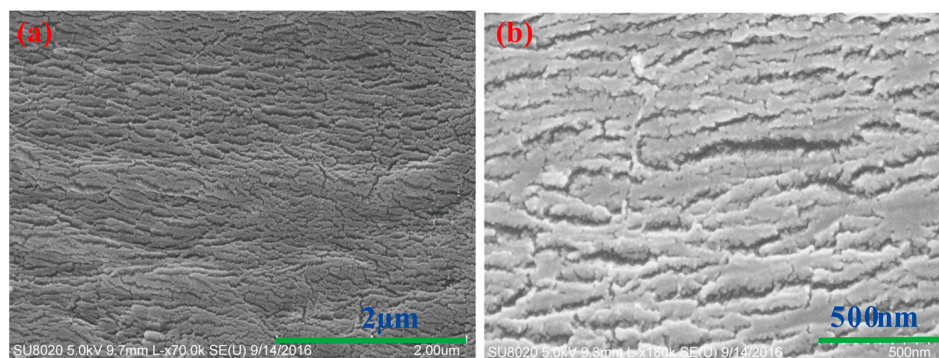


Figure 2. Scanning electron microscope of PTFE film to show the roughness: (a) the tribo-contact surface; (b) the surface with a relative smaller area.

As shown in Figures 3a and 4a, when the system is subjected to a low frequency vibration, the low frequency oscillator will vibrate with multiple impacts to the PTFE film on the cantilever, resulting in voltage and current output from a single CB electrode. At the same time, the periodical multiple

impacts on the cantilever drive the pick-up coil to oscillate with a much high frequency vibration in the electromagnetic field (see Figures 3b and 4b). The magnetic flux linkage in the coil and magnet were obtained via a finite element analysis (FEA) simulation performed by COMSOL Multiphysics and is illustrated in Figure 5. The change rate of the magnetic flux can be clearly observed in Figure 5a,b. Thus, a current is generated because of the coil with relative motion in the magnetic field. We assume that the weight of the cantilever m_1 is concentrated at the free edge. We used x_1 and x_2 to denote the tip displacement and the displacement of the triboelectric impact, respectively. Then we obtained

$$m_1 \ddot{x}_1 = -c_1 \dot{x}_1 - m_1 A \omega^2 \sin(\omega t) + F_2 + F_3 + F_{ele} \tag{1}$$

$$m_2 \ddot{x}_2 = -k_2 x_2 - c_2 \dot{x}_2 - m_2 A \omega^2 \sin(\omega t) + F_1 \tag{2}$$

where c_1 and c_2 are the damping effect, and ω and A are the excitation vibration parameters. F_1 is the triboelectric contact force acting on the mass m_2 by the cantilever. F_2 and F_3 are the acting tip force from m_2 and the constraint displacement force by magnetic position, respectively. F_{ele} is the force on the coil from the electromagnetic field. Supposing the bending moment is M , EI is the flexural rigidity of the cantilever. Using engineering beam bending theory and the principle of superposition [31], we can obtain

$$x_1 = x_2 + \Delta_3 + \theta_a b = x_2 + \left[-\frac{(F_1 + F_2)a^2}{2EI} - \frac{F_2 b a}{EI} \right] b - \frac{F_2 b^3}{3EI}. \tag{3}$$

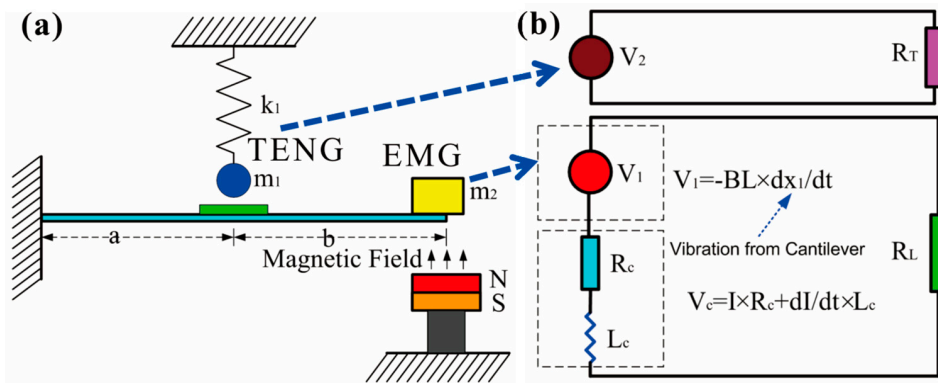


Figure 3. (a) Oscillators in intermittent multiple triboelectric impacts to the PTFE film on the cantilever; (b) the equivalent circuit of the TENG and EMG.

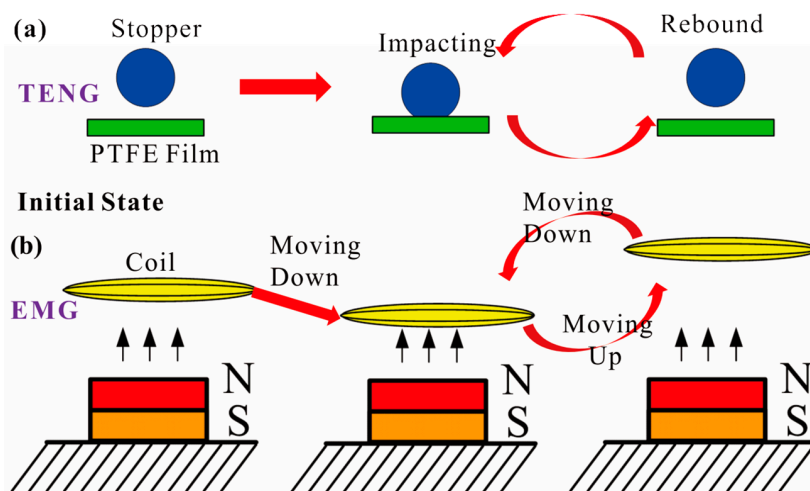


Figure 4. Working principle of the hybrid TENG and EMG multi-impacts energy harvester based on the cantilever beam: (a) TENG; (b) EMG.

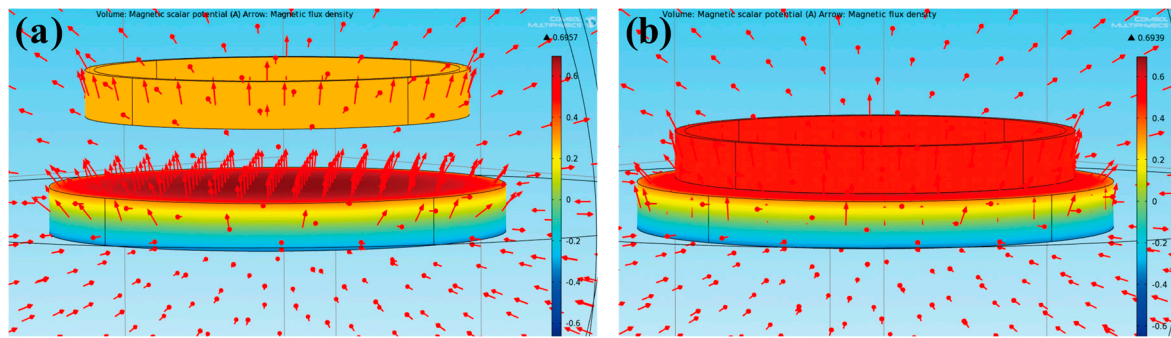


Figure 5. The magnetic flux linkage between magnet and coil: (a) FEA simulation of magnetic flux with a 2 mm gap; (b) FEA simulation of magnetic flux with a smaller gap.

If the contact force is negative, mass m_2 does not make contact with the cantilever beam. Therefore, $F_1 = 0$, and $F_2 = -\frac{3EI}{(a+b)^3}x_3$. If x_1 is smaller than -2 mm, F_3 presents a substantial value, which indicates an instantaneous bounce-back. The generated power P_{em} of the EMG is as follows:

$$P_{em} = R_L \left(\frac{B_d \sum A_c \dot{x}_1}{R_c + j\omega L_c + R_L} \right)^2 \quad (4)$$

where R_c and L_c are the resistor and the total length of the coil, respectively. A_c is the effective area of the coil. B_d is the magnetic flux coefficient in the vertical direction. Keep in mind that the magnetic flux is nonlinear surrounding the pick-up coil. As for the TENG component, when contact occurs between the copper electrode piece and the PTFE film, the voltage from the single CB electrode triboelectric is given as [32]

$$V_{oc} = \frac{Q_{sc}}{C} = \frac{2\sigma x_2}{\epsilon_0}. \quad (5)$$

The displacement of proof mass is found to be linear with the triboelectric output voltage. Thus, the acceleration is linearly related to triboelectric output voltage based on Hook's law. Thus, with a fierce impact on the cantilever beam, a larger output voltage can be obtained from the TENG.

3. Results and Discussion

Figure 6 depicts the schematic of the experimental setup system for TENG and EMG based on the cantilever beam. A shaker (VT-500, Dongguan Aisali Equipment Company, Dongguan, China), a function generator (Stanford Research System DS345, Stanford company, Sunnyvale, CS, USA), an oscilloscope, and an electrometer (Keithley 6514) were used for the electrical performance tests. The system parameters are given in Table 1. The function generator was used to provide the input power source, and the oscilloscope was used to measure the output voltage on the resistors of EMG. The electrometer was adopted to measure the open-circuit voltage and external load impedance from the TENG. When the hybrid TENG and EMG was subjected to a wideband low frequency vibration from the shaker, the low-frequency oscillator responded first with motion at low frequencies. The thick metallic copper piece then made triboelectric impact with the PTFE compound film, which resulted in the power flowing along the single CB electrode. At the same time, the high frequency cantilever would oscillate, resulting in an electrical current flowing through the coil in the electromagnetic field. To estimate the response 3 db bandwidth, the system was characterized by an excitation frequency from 10 Hz to 45 Hz under sinusoidal excitations with a constant acceleration (1 g and 2 g) across the load resistor (40 Ω) for an excitation frequency. It was observed that the 3 db bandwidth of the EMG was 12–35 Hz. The average of the power generated in the 3 db range was calculated with a number value 38.1 $\mu\text{W}/\text{m}^2$ with the 2 g vibration amplitude in EMG. With a higher frequency, it showed weaker impacts in Figure 7a,b from TENG. The open-circuit voltage and short-circuit current at a 2 g

amplitude was two times greater than those at a 1 g amplitude in this case. It is interesting that two peaks (20 Hz and 30 Hz) in EMG occurred within 10–45 Hz at 1 g and 2 g (see Figure 7c). As shown in Figure 7d, the measured power across the load resistor can reach up to maximum powers of 52 μW and 37 μW at 20 Hz under excitations of 1 g and 2 g, respectively. Figure 8 depicts an approximately quadratic relationship for vibration amplitude and the output voltage of TENG and EMG, respectively. The average power across the external load resistor obtained from TENG is shown in Figure 9 with a maximum power of 30 $\mu\text{W}/\text{m}^2$. The force value of the impact was calculated by the numerical simulation shown in Figure 10.

The instantaneous short-circuit current from TENG with different excitations shown in Figure 11 can be used to demonstrate the nonlinear dynamic impact phenomena. Figure 11a–c describe a measured short-circuit current (I_{sc}) with increasing frequency and the same amplitude. The bouncing state of the TENG showed complicated phenomena. The top sharp curve meant the oscillator impact, and the bottom sharp curve meant the impact of the free tip. Compared with Figure 11b,d, we found that the larger the amplitude was, the fiercer the bouncing was. Figure 12 depicts the dynamic response of EMG. Note that the bottom sharp curve meant the strong nonlinear impact from the magnetic. After each impact, the free tip of the cantilever would vibrate with a much higher frequency, which was close to the oscillator's resonant frequency. The bottom sharp shape indicated a strong impact between the tip cantilever and the magnetic stopper.

Table 1. System parameters.

Modeling Parameters	Symbols	System	Unit
Cantilever Beam Length	L	6	cm
Cantilever Beam Width	W	2	cm
Cantilever Beam Thickness	H	1	mm
Young's Module	E	3	GPa
Oscillator Resonant Frequency	f_1	8	Hz
Cantilever Resonant Frequency	f_2	74.5	Hz
Coil Turns	N	100	1
Coil Mass	m	2.1	g
Coil Resistance	R_c	40	Ω
Load Resistance	R_l	40	Ω
Oscillator Mass	m_1	1.9	g
Magnetic Flux	B	0.695	T
Magnetic Flux Coefficient on y	c_m	0.0175	T/mm

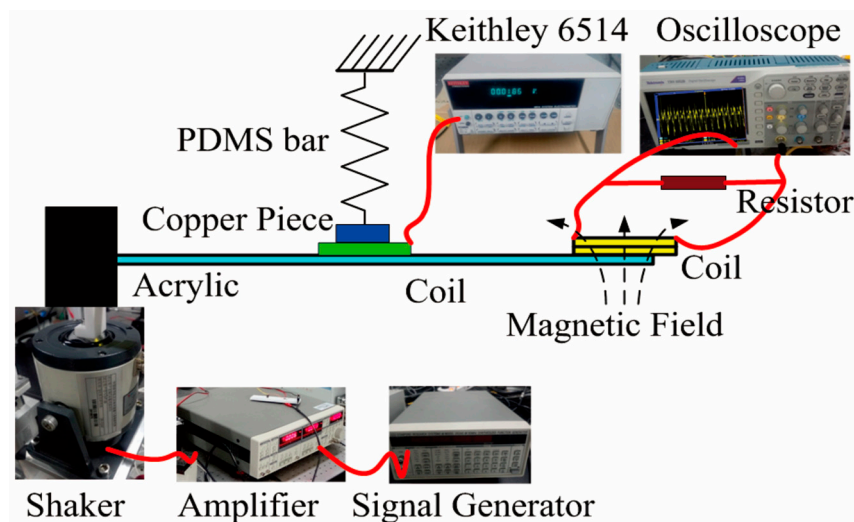


Figure 6. The schematic of the experimental setup for a hybrid TENG and EMG system.

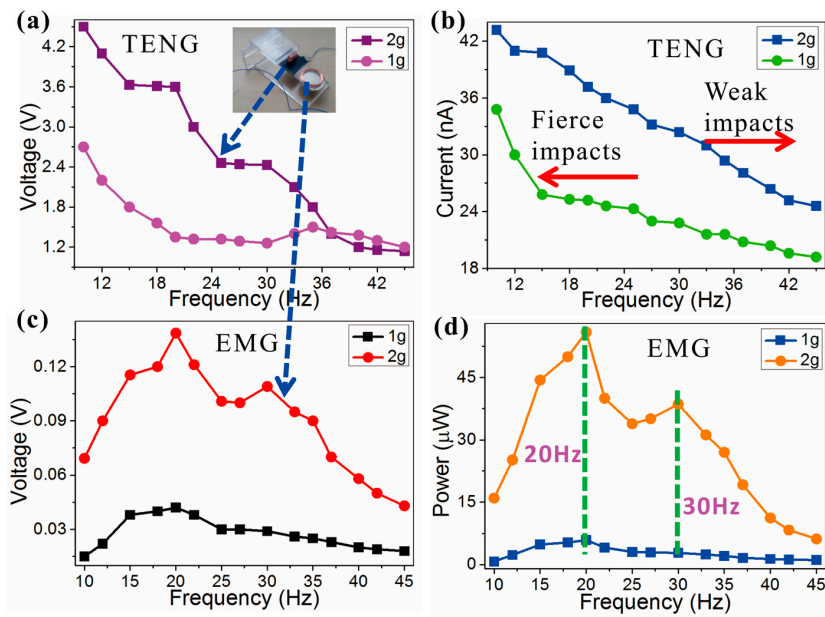


Figure 7. Measurement results as a function of frequency and different excitations: (a) the maximum open-circuit voltage of TENG; (b) the short-circuit current of TENG; (c) the maximum voltage on load resistor from EMG; (d) the harvested power from EMG.

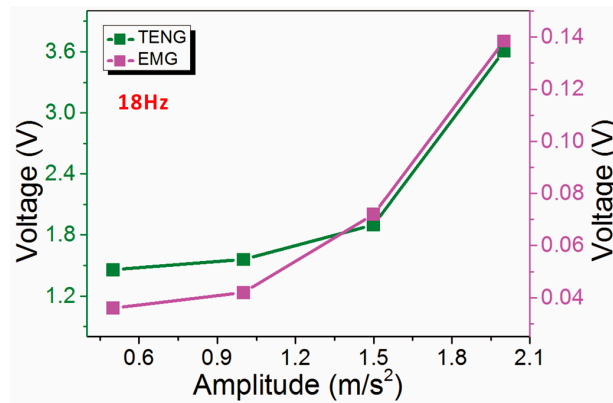


Figure 8. Numerical relationship for vibration amplitude and the output voltage of TENG and EMG, respectively.

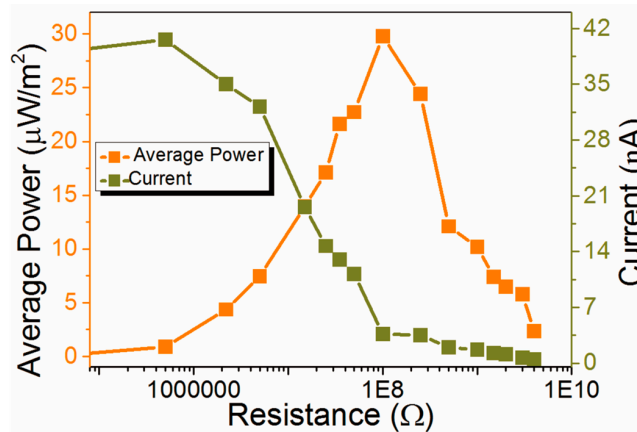


Figure 9. The generated power based on the different load resistors from TENG.

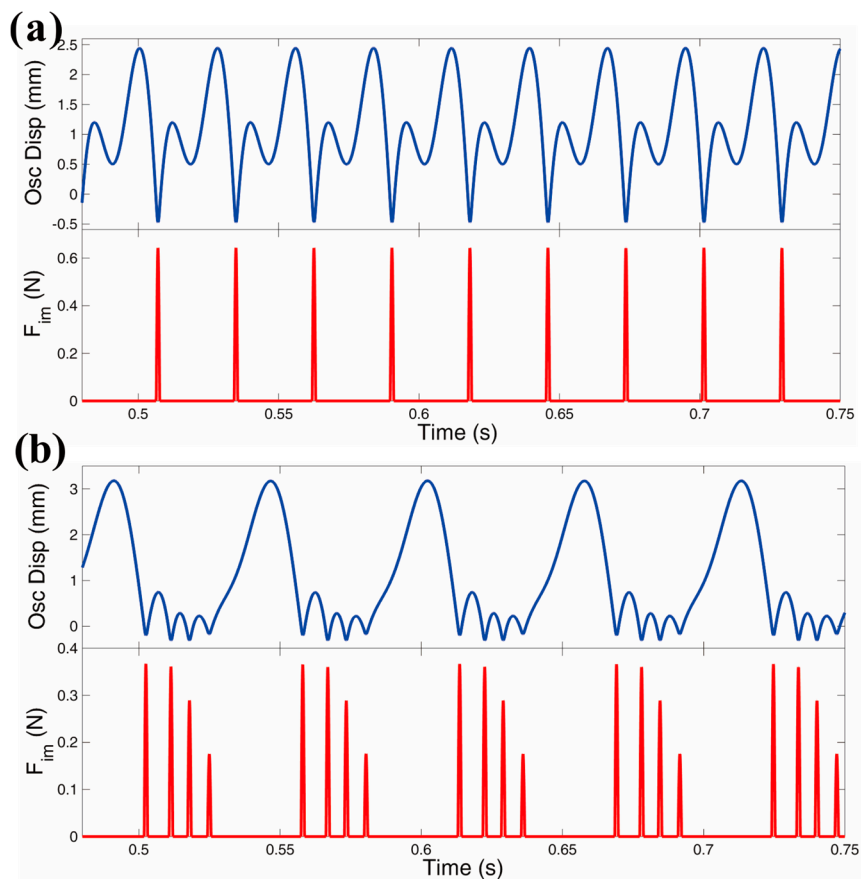


Figure 10. Numerical simulation results: (a) 18 Hz, 2 g, fierce impact; (b) 36 Hz, 2 g, weak impacts. Note that the second panel is the impact force F_{im} from the oscillator.

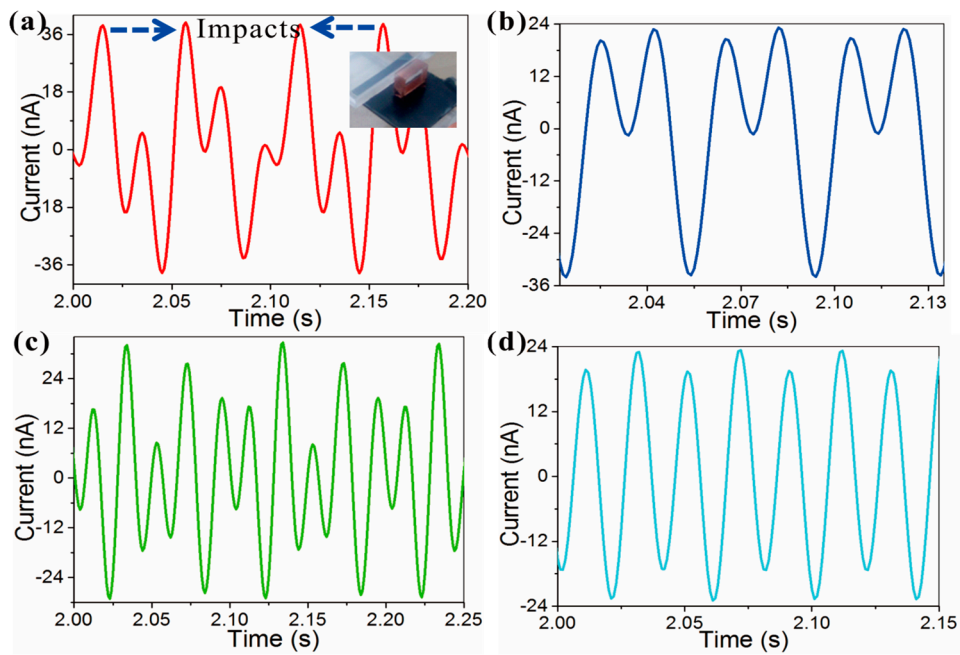


Figure 11. Measurement current of TENG: (a) 20 Hz, 2 g; (b) 25 Hz, 2 g; (c) 30 Hz, 2 g; (d) 25 Hz, 1 g.

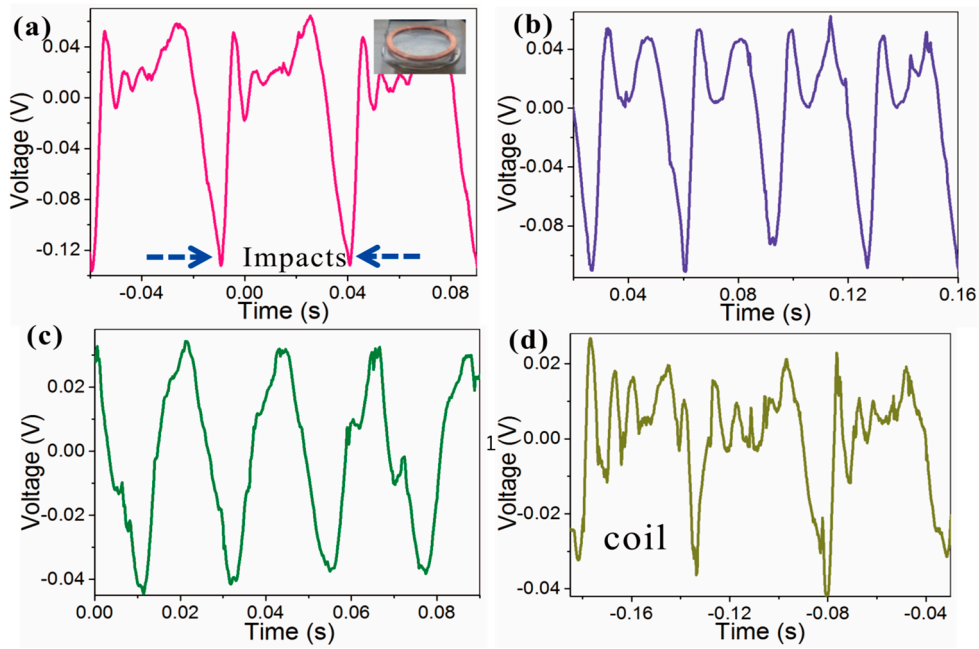


Figure 12. Measured voltage of EMG: (a) 18 Hz, 2 g; (b) 20 Hz, 2 g; (c) 24 Hz, 2 g; (d) 18 Hz, 1 g.

To validate the measurement results, the numerical simulation using MATLAB based on the equations mentioned above was analyzed. Note that the first and second panels shown in Figure 13 represent the displacement of the TENG oscillators and tip cantilever, respectively. It is obvious that the nonlinearity was caused by the intermittent TENG contact and the tip constrained space from magnet. Compared with the measurement voltage results (see Figure 14b) and the numerical simulation results (see Figure 14b), we found that the voltage output was in good agreement under an excitation of 18 Hz and 1 g.

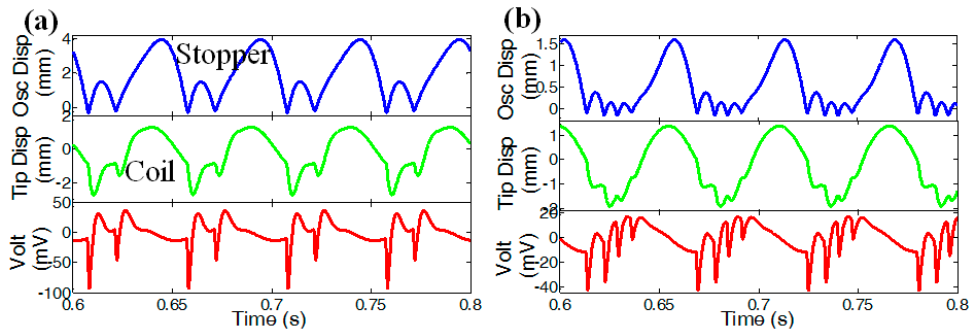


Figure 13. Numerical simulation result: (a) 20 Hz, 2 g; (b) 18 Hz, 1 g.

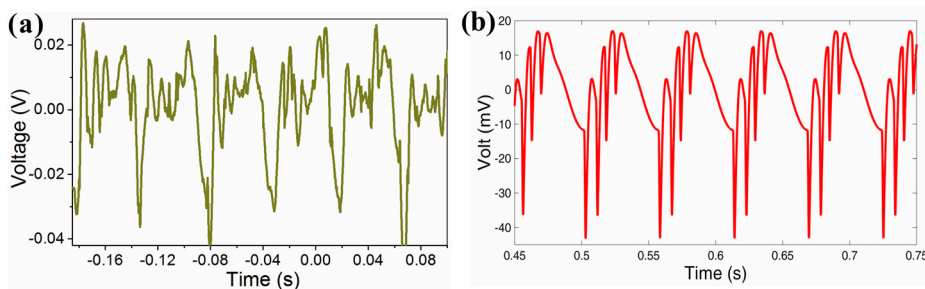


Figure 14. (a) The experimental test result and (b) the numerical simulation result, 18 Hz, 1 g. Note that the voltages in both figures were from the coil of EMG.

4. Conclusions

We have demonstrated the feasibility of a hybrid EMG and TENG system using a multi-impact approach for broad-bandwidth-frequency (10–45 Hz) energy harvesting. The mathematical model included an oscillator that can have impacts on the cantilever and the nonlinear Lorenz force that comes from the motion of the coil in the electromagnetic field. Due to the nonlinearity of the impact and the constraint space, the dynamic response of the cantilever had a much broader bandwidth, with two peaks (20 Hz and 30 Hz) between its oscillator resonant frequencies and several times of the oscillator resonant frequencies. Moreover, the dynamic responses in the hybrid EMG and TENG were analyzed, and we found that the experimental results and the numerical simulation results were in good agreement.

Acknowledgments: This study was funded by No. 20160825153358948 from Shenzhen Science and Technology Innovation Committee.

Author Contributions: Jianxiong Zhu conceived and designed the experiments. Haibing Hu and Hua Zhu analyzed the data and performed the simulations. Aochen Wang and all the authors helped to write the paper.

Conflicts of Interest: The authors declare no conflicts of interest with this publication.

References

1. Ando, B.; Baglio, S.; Trigona, C.; Dumas, N.; Latorre, L.; Nouet, P. Nonlinear mechanism in MEMS devices for energy harvesting applications. *J. Micromech. Microeng.* **2010**, *20*, 125020. [[CrossRef](#)]
2. Younis, M.I.; Ouakad, H.M.; Alsaleem, F.M.; Ronald Miles, M.; Cui, W. Nonlinear dynamics of MEMS arches under harmonic electrostatic actuation. *J. Microelectromech. Syst.* **2010**, *19*, 647–656.
3. Kim, J.E.; Kim, Y.Y. Power enhancing by reversing mode sequence in tuned mass-spring unit attached vibration energy harvester. *AIP Adv.* **2013**, *3*, 072103. [[CrossRef](#)]
4. Qiu, J.; Feng, Z.C. Parameter dependence of the impact dynamics of thin plates. *Comput. Struct.* **2000**, *75*, 491–506. [[CrossRef](#)]
5. Umeda, M.; Nakamura, K.; Ueha, S. Analysis of the transformation of mechanical impact energy to electric energy using piezoelectric vibrator. *Jpn. J. Appl. Phys.* **1996**, *35*, 3267–3273. [[CrossRef](#)]
6. Yang, Y.; Zhang, H.; Zhong, X.; Yi, F.; Yu, R.; Zhang, Y.; Wang, Z.L. Electret film enhanced triboelectric nanogenerator matrix for self-powered instantaneous tactile imaging. *ACS Appl. Mater. Interfaces* **2014**, *6*, 3680–3688. [[CrossRef](#)] [[PubMed](#)]
7. Zhang, X.; Wu, L.; Sessler, G.M. Energy harvesting from vibration with cross-linked polypropylene piezoelectrets. *AIP Adv.* **2015**, *5*, 077185. [[CrossRef](#)]
8. Zhang, W.M.; Meng, G.; Wei, K.X. Dynamics of nonlinear coupled electrostatic micromechanical resonators under two-frequency parametric and external excitations. *Shock Vib.* **2010**, *17*, 759–770. [[CrossRef](#)]
9. Li, S.; Crovetto, A.; Peng, Z.; Zhang, A.; Hansen, O.; Wang, M.; Wang, F. Bi-resonant structure with piezoelectric PVDF films for energy harvesting from random vibration sources at low frequency. *Sens. Actuators A Phys.* **2016**, *247*, 547–554. [[CrossRef](#)]
10. Helseth, L.E.; Guo, X.D. Triboelectric motion sensor combined with electromagnetic induction energy harvester. *Sens. Actuators A* **2016**, *246*, 66–72. [[CrossRef](#)]
11. Berdy, D.F.; Srisungsitthisunti, P.; Jung, B.; Xu, X.; Rhoads, J.F.; Peroulis, D. Low-frequency meandering piezoelectric vibration energy harvester. *IEEE Trans. Ultrason. Ferroelectr. Freq. Control* **2012**, *59*, 846–858. [[CrossRef](#)] [[PubMed](#)]
12. Challa, V.R.; Prasad, M.G.; Shi, Y.; Fisher, F.T. A vibration energy harvesting device with bidirectional resonance frequency tunability. *Smart Mater. Struct.* **2008**, *17*, 015035. [[CrossRef](#)]
13. Chen, L.; Jiang, W. A piezoelectric energy harvester based on internal resonance. *Acta Mech. Sin.* **2015**, *31*, 223–228. [[CrossRef](#)]
14. Abed, I.; Kacem, N.; Bouhaddi, N.; Bouazizi, M.L. Multi-modal vibration energy harvesting approach based on nonlinear oscillator arrays under magnetic levitation. *Smart Mater. Struct.* **2015**, *25*, 025018. [[CrossRef](#)]

15. Olszewski, O.Z.; Houlihan, R.; Mathewson, A.; Jackson, N. A low frequency MEMS energy harvester scavenging energy from magnetic field surrounding an AC current-carrying wire. *J. Phys. Conf. Ser.* **2016**, *757*, 012039. [[CrossRef](#)]
16. Yang, B.; Lee, C. Non-resonant electromagnetic wideband energy harvesting mechanism for low frequency vibrations. *Microsyst. Technol.* **2010**, *16*, 961–966. [[CrossRef](#)]
17. Yuksek, N.S.; Feng, Z.C.; Almasri, M. Broadband electromagnetic power harvester from vibrations via frequency conversion by impact oscillations. *Appl. Phys. Lett.* **2014**, *105*, 113902. [[CrossRef](#)]
18. Salauddin, M.; Halim, M.A.; Park, J.Y. A magnetic-spring-based, low-frequency vibration energy harvester comprising a dual halfbach array. *Smart Mater. Struct.* **2016**, *25*, 095017. [[CrossRef](#)]
19. Jung, S.M.; Yun, K.S. Energy-harvesting device with mechanical frequency-up conversion mechanism for increased power efficiency and wideband operation. *Appl. Phys. Lett.* **2010**, *96*, 111906. [[CrossRef](#)]
20. Mahmoudi, S.; Kacem, N.; Bouhaddi, N. Enhancement of the performance of a hybrid nonlinear vibration energy harvester based on piezoelectric and electromagnetic transductions. *Smart Mater. Struct.* **2014**, *23*, 075024. [[CrossRef](#)]
21. Guo, H.; Wen, Z.; Zi, Y.; Yeh, M.H.; Wang, J.; Zhu, L.; Wang, Z.L. A water-proof triboelectric-electromagnetic hybrid generator for energy harvesting in harsh environments. *Adv. Energy Mater.* **2016**, *6*, 1501593. [[CrossRef](#)]
22. Han, M.; Zhang, X.; Liu, W.; Sun, X.; Peng, X.; Zhang, H. Low-frequency wide-band hybrid energy harvester based on piezoelectric and triboelectric mechanism. *Sci. China Technol. Sci.* **2013**, *56*, 1835–1841. [[CrossRef](#)]
23. Halim, M.A.; Park, J.Y. Piezoceramic based wideband energy harvester using impact-enhanced dynamic magnifier for low frequency vibration. *Ceram. Int.* **2015**, *41*, S702–S707. [[CrossRef](#)]
24. Halim, M.A.; Khym, S.; Park, J.Y. Frequency up-converted wide bandwidth piezoelectric energy harvester using mechanical impact. *J. Appl. Phys.* **2013**, *114*, 044902. [[CrossRef](#)]
25. Halim, M.A.; Kim, D.H.; Park, J.Y. Low frequency vibration energy harvester using stopper-engaged dynamic magnifier for increased power and wide bandwidth. *J. Electr. Eng. Technol.* **2016**, *11*, 707–714. [[CrossRef](#)]
26. Fan, F.R.; Tang, W.; Yao, Y.; Luo, J.; Zhang, C.; Wang, Z.L. Complementary power output characteristics of electromagnetic generators and triboelectric generators. *Nanotechnology* **2014**, *25*, 135402. [[CrossRef](#)] [[PubMed](#)]
27. Zhang, K.W.; Wang, X.; Yang, Y.; Wang, Z.L. Hybridized electromagnetic–triboelectric nanogenerator for scavenging biomechanical energy for sustainably powering wearable electronics. *ACS Nano* **2015**, *9*, 3521–3529. [[CrossRef](#)] [[PubMed](#)]
28. Salauddin, M.; Park, J.Y. A handy motion driven hybrid energy harvester: Dual halfbach array based electromagnetic and triboelectric generators. *J. Phys. Conf. Ser.* **2016**, *773*, 012004. [[CrossRef](#)]
29. Gupta, R.K.; Shi, Q.F.; Dhakar, L.; Wang, T.; Heng, C.H.; Lee, C.K. Broadband energy harvester using Non-linear polymer spring and electromagnetic/triboelectric hybrid mechanism. *Sci. Rep.* **2017**, *7*, 41396. [[CrossRef](#)] [[PubMed](#)]
30. Salauddin, M.; Rasel, M.; Kim, J.W.; Park, J.Y. Design and experiment of hybridized electromagnetic-triboelectric energy harvester using halfbach magnet array from handshaking vibration. *Energy Convers. Manag.* **2017**, *153*, 1–11. [[CrossRef](#)]
31. Hassan, O.A. A simplified structural analysis of statically indeterminate continuous thick beams. *Int. J. Mech. Eng. Educ.* **2016**, *44*, 257–271. [[CrossRef](#)]
32. Niu, S.M.; Wang, S.H.; Lin, L.; Liu, Y.; Zhou, Y.S.; Hua, Y.F.; Wang, Z.L. Theoretical study of contact-mode triboelectric nanogenerators as an effective power source. *Energy Environ. Sci.* **2013**, *6*, 3576–3583. [[CrossRef](#)]

